Journal of Natural Gas Science and Engineering 104 (2022) 104674

Contents lists available at ScienceDirect

Journal of Natural Gas Science and Engineering

journal homepage: www.elsevier.com/locate/jngse

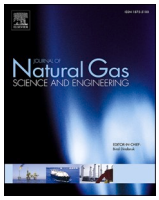

Investigation on reactive flow through porous media by quadtree Lattice Boltzmann☆

Sadegh Mahmoudi [a], Shahab Ayatollahi [a], Saeid Jamshidi [a,*], Amir Raoof [b]

[a] Department of Chemical and Petroleum Engineering, Sharif University of Technology, Iran
[b] Department of Earth Sciences, Utrecht University, the Netherlands

ARTICLE INFO

Keywords:
Lattice Boltzmann method
Reactive flow
Quadtree
Grid refinement
Mass transfer coefficients

ABSTRACT

In this study, in order to investigate the effect of the underlying pore-scale processes on continuum scale simulations of porous media dissolution, we improve the standard Lattice Boltzmann method using Quadtree grid refinement approach to simulate fluid flow and reactive transport through large domain sizes. Our results have shown considerable computational improvements up to 80% in simulation time together with increased numerical accuracy. The results and the added value of the new approach are discussed using comparison of our model with the conventional LBM. Moreover, we have applied a systematic analysis by increasing complexity levels and starting from fluid flow and continuing with tracer transport and reactive transport in single pores, and ultimately, reactive transport in dissolving porous structures. For each case, the accuracy and computational benefits of the Quadtree models are discussed and dimensionless numbers are used to characterize regimes of flow and reaction in each step of comparison. Porosity-permeability variation in a 2D pore structure and mass transfer coefficient in a closed-end fracture with porous walls are then evaluated under different flow conditions.

1. Introduction

In oil and gas reservoirs, the reactive flow during the acidizing process changes the rock pore structure and affects the flow conditions. In continuum-scale modelling of such processes, the presence of a large concentration gradient at the vicinity of the rock grains and the continuous changes in rock-fluid interfaces of the porous medium conflicts with the continuum assumption. Therefore, the need for pore scale modelling is evident for the effective local mass transport and molecular diffusion coefficients. Over the last decade, pore scale studies have received considerable attention in scientific communities as well as industrial applications. They provide opportunities to understand flow and transport mechanisms that are operating at the pore scale and how they control the macroscopic behaviour of porous media. Liu et al., (2021), and Jiang and Xu (2021) are examples of studies that used Lattice Boltzmann method (LBM) to investigate pore-scale mechanisms of enhanced oil recovery (EOR) and the applications related to reactive fluid flow in porous media such as CO_2 injection. Zhang et al., (2021) developed a geochemical lattice Boltzmann model to model multi-component reaction flow in porous media. Vasheghani Farahani et al., (2020) investigated heat transfer in multi-phase systems of porous media by LBM and Soleimani et al., (2019) studied the effect of the gas condensate drop-out on the gas relative permeability values using LBM.

Lattice Boltzmann Method as a meso-scale approach is a numerical solver for Navier-Stokes (NSE) and Convection-Diffusion (CDE) equations for slightly compressible flow with a second-order accuracy. LBM provides simple approaches for simulation of reactive transport with complex chemistry. Knutson et al., (2001) investigated pore scale heterogeneities and dissolution effects on mass transfer coefficient. They used LBM to simulate water flow and solute transport from distributed non-aqueous phase liquids in a two-dimensional porous media. Kang et al., (2002) proposed a LB model to simulate chemical dissolution in porous media. Kang et al. (2014), Yoon et al., (2015) and Min et al., (2016) studied the induced change in porosity and permeability of porous media by implementing LBM to simulate pore scale dissolution and precipitation. More recently, Montemore et al., (2017) used LB models to investigate reactive transport in nano-porous catalysts and catalytic performances. Gao et al., (2017) proposed a geochemical numerical model for pore scale reactive transport using LB models and investigated reactive fluid transport in 3D porous media with different

☆ The Authors declare that this manuscript is original work, not published elsewhere or under consideration for publication elsewhere and all authors have seen the manuscript and agree to its submission to Computers and Chemical Engineering.

* Corresponding author.
E-mail address: jamshidi@sharif.edu (S. Jamshidi).

https://doi.org/10.1016/j.jngse.2022.104674
Received 10 April 2022; Received in revised form 31 May 2022; Accepted 13 June 2022
Available online 25 June 2022

reactive mineral surfaces. On the other hand, there are some studies that used a combination of LBM with other numerical methods like Direct Numerical Simulation (DNS) or particle tracking (PT) for studying reactive or active transport phenomena in porous media. LBM in these cases often is used to simulate fluid flow whereas DNS based on finite-volume is used to compute concentration fields for reactive transport in porous media (Yoon et al., 2012; Chen et al., 2013; Tong and He, 2015) and PT is used to compute the transport of particles and subsequent deposition or retention (Parvan et al., 2020; Kermani et al., 2020).

Although the applications of LBM for flow in porous media mainly deal with high resolution of individual grains at the pore scale, but also there have been some efforts to extend the simulation domain to larger scale. By this approach, pore scale properties may be utilized as the continuum scale parameters by upscaling the pore scale results (Lichtner and Kang, 2007). It is very well established that LBM can take advantage of high degree of parallelism, and scale up on thousands cores. (Succi et al., 2019). Besides, LBM can also benefit from the powerful local grid refinement approaches that focused on grid density near and/or far from solid faces or boundary conditions to increase the computational efficiency and attain larger simulation domain size. Quadtree grid refinement, as a type of unstructured grid, is constructed by recursive subdivision of an initial domain based on a predefined criterion and results in square cells of different sizes. Some of the advantages of Quadtree grid refinement such as locally high-resolution grids, automatic mesh generation, simple hierarchical data structures and dynamically adaptive grids have made it popular in recent years. Crouse et al., (2003) adapted LBM on Quadtree grids using the method of Filippova and Hänel (1998). Originally, Crouse et al., 2003 developed the Quadtree LBM based on mesh centred grids and integrated it with a linear interpolation for treating the interface. Chen et al., (2011) and, Zhang et al., (2016), used Quadtree grids to simulate flow of fluid in multiscale porous media. They also adopted the linear interpolation of Crouse et al., (2003), but used a back-forth error compensation-correction (BEFECC) scheme to achieve second-order accuracy. Yu and Fan (2009) also adopted Quadtree grids to simulate a bubble rising in a viscous fluid using cell centred approach. Cell centred Quadtree is based on the scheme developed by Chen et al., (2006) and is mass conservative, simple in application, and does not need interpolation or change in non-equilibrium density distribution function. Foroughi et al., (2013) also implemented cell-centred approach and volumetric distribution transfer method to simulate fluid flow in porous media. Their LB model is integrated with an image reconstruction algorithm based on Quadtree grids. Their results revealed that Quadtree is in good agreement with the regular uniform LB method and FEM. They also showed that Quadtree decreases the simulation time significantly compared with the regular uniform LB method.

In this work, we constructed a reactive LBM on Quadtree meshes for the first time using the cell centred approach and discusses the advantages of the scheme. The D2Q9 Linear Bhatnagar Gross and Krook (LBGK) model is implemented for both fluid flow and solute concentration to study reactive systems. To the authors' knowledge there is no other similar work in the literature that studied the reaction and dissolution of porous media by Quadtree method. The organization of this manuscript goes as follows; first, the LB formulation is briefly introduced and its application on Quadtree meshes is described. Several validation examples are then presented. Next, the simulation results of Quadtree LBM for reactive flow through porous media are discussed as a novel technique for this complex case. Furthermore, large domain size 2D pore structures were considered to simulate porosity-permeability variation during reactive flow and to investigate the mass transfer coefficients.

2. Modelling flow and reactive transport using LBM

In simulating reactive transport, it is commonly assumed that the effect of concentrations on flow properties are negligible. Using this assumption, the CDE and NSE are decoupled and are represented using separate sets of distribution functions in LBM (Ponce Dawson et al., 1993). Therefore, the velocity field relates the flow domain and the concentration domain through the equilibrium distribution function.

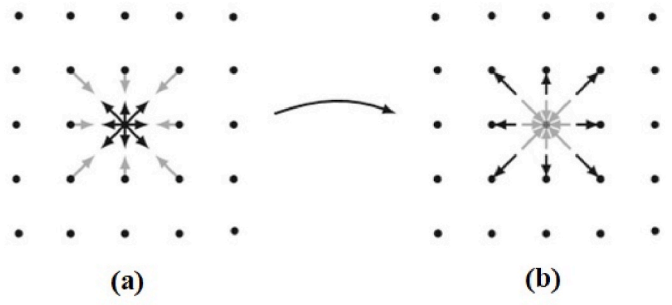

Fig. 1. D2Q9 model, a) represents the collision and b) shows the streaming step.

In order to approximate the solution of NSE, the LBGK collision form of Lattice Boltzmann Equation (LBE) is used to obtain the flow field distribution:

$$f_i(x+\vec{e_i}\Delta t, t+\Delta t) - f_i(x,t) = -\Delta t / \tau (f_i(x,t) - f_i^{eq}(\rho, \vec{u}^{eq})) + \Delta t F_i \quad \text{Eq. (1)}$$

where f_i is the directional distribution function, f_i^{eq} represents equilibrium distribution function, e_i is directional lattice velocity and τ is the relaxation time. u^{eq} is the equilibrium velocity, $\rho = \sum f_i$ is the fluid density, and F_i represents possible source and sink effects. In Eq. (1) the term before F_i on the right hand side represents the collision operator and the left hand side term operates as streaming of the distributions.

Fig. 1 shows the collision and streaming steps in D2Q9 LB models that utilize 2D lattices and perform with 9 lattice velocities. For D2Q9 model f^{eq} is determined by:

$$f_i^{eq}(x) = w_i \rho \left[1 + \frac{\vec{e_i}.\vec{u}^{eq}}{c_s^2} + \frac{(\vec{e_i}.\vec{u}^{eq})^2}{2{c_s}^4} - \frac{(\vec{u}^{eq})^2}{2{c_s}^2} \right] \quad \text{Eq. (2)}$$

In Eq. (2) w_i is the directional weight factor and c_s is the lattice speed of sound.

Guo et al., (2002), provided a scheme for incorporation of an external force term, F, where flow velocity is modified to partially contribute to the applied body force and therefore, the equilibrium velocity u^{eq} is:

$$\vec{u}^{eq} = \vec{u} + \frac{\vec{F}\Delta t}{2\rho} = 1 \Big/ \rho \sum \vec{e_i} f_i + \frac{\vec{F}\Delta t}{2\rho} \quad \text{Eq. (3)}$$

This form of the velocity may be interpreted as averaging velocity before and after the forcing terms to guarantee the accuracy of the second-order space-time terms (Krüger et al., 2017). Furthermore, the source/since term F_i is calculated by Eq. (4):

$$F_i = w_i \left(1 - \frac{1}{2\tau}\right) \left(\frac{\vec{e_i} - \vec{u}}{c_s^2} + \frac{(\vec{e_i}.\vec{u})\vec{e_i}}{c_s^4} \right) . \vec{F} \quad \text{Eq. (4)}$$

To calculate the concentration field, the collision operator is defined as the sum of a source term and a nonreactive term, which provide:

$$g_i(x+\vec{e_i}\Delta t, t+\Delta t) - g_i(x,t) = -\Delta t / \tau_s (g_i(x,t) - g_i^{eq}(C, \vec{u}^{eq})) + \Delta t S_i. \quad \text{Eq. (5)}$$

In Eq. (5) g_i is the directional concentration distribution function, τ_s is the relaxation time for the concentration domain, C is the concentration at any point ($C = \sum g_i$) and g_i^{eq} is the equilibrium distribution function which for D2Q9 model is calculated by:

$$g_i^{eq}(x) = w_i C\left[1 + \frac{\vec{e_i}.\vec{u}^{eq}}{{c_s}^2} + \frac{(\vec{e_i}.\vec{u}^{eq})^2}{2{c_s}^4} - \frac{(\vec{u}^{eq})^2}{2{c_s}^2}\right] \quad \text{Eq. (6)}$$

Since the concentration is a scalar field and the collision term on right hand side of Eq. (5) does not conserve the momentum, the computational efficiency may be enhanced by considering the linear velocity terms of the equilibrium distribution function (i.e., the D2Q4 model; as it is implemented in studies like: Knutson et al., 2001, Zhang et al., 2002, Jiménez-Hornero et al., 2004 and Kang et al., 2007). However, the four-speed model brings some drawbacks and affects the numerical accuracy and convergence. This issue has been analysed by Li et al., (2017) and Krüger et al., (2017). Krüger et al., (2017) provided a detailed discussion on the diffusion coefficient stated that the D2Q4 diffusion coefficient is velocity dependent and the diffusion coefficient in D2Q9 model is smaller than the D2Q4 model under similar conditions. As a result, this smaller diffusion results in higher Peclet and Damköhler numbers. In the present work, we have implemented the D2Q9 model to both flow and concentration calculations.

The term S_i in Eq. (5) represents possible source and sinks which originally account for homogeneous reactions. For heterogeneous reactions, the reaction boundary condition at the solid boundaries can be replaced with a reaction term at the computational nodes adjacent to the solid nodes. Patel et al., (2014) adopted this approach by coupling an external operator (i.e., geochemical solver PHREEQC). Therefore, the heterogeneous reactions at the solid-fluid interface are considered as pseudo-homogeneous reactions by including an additional source (collision) term. The reaction term can be expressed as (Krüger et al., 2017):

$$S_i = \left(1 - \frac{1}{2\tau_s}\right) w_i \kappa (C_s - C) \quad \text{Eq. (7)}$$

where κ is the average rate constant with first order kinetics and C_s is the equilibrium concentration.

In LBM application, the common practice is to implicate the diffusion coefficient and kinematic viscosity through dimensional analysis, to determine the relaxation times through similar equations, $D_m = c_s^2\left(\tau_s - \frac{\Delta t}{2}\right)$ and $\upsilon = c_s^2\left(\tau - \frac{\Delta t}{2}\right)$ respectively.

Schmidt and Sherwood dimensionless numbers are often used to characterize mass transfer in porous media. The Schmidt number (Sc) is defined as the ratio of kinematic viscosity (i.e., momentum diffusivity) to mass diffusivity and characterizes momentum and mass diffusion convection processes. The Sherwood number (Sh) which is defined as the ratio of advection to diffusion mass transfer, can be estimated using the relation proposed by Yoshino and Inamuro (2003) with some modification as:

$$Sh = \frac{\Delta C_\sigma}{\left(C_{\sigma|b}\right)_{in} - \left(C_{\sigma|w}\right)_{out}} \mathrm{Re} Sc^{1/3} \frac{L}{S_{total}} \quad \text{Eq. (8)}$$

where $C_{\sigma|b}$ and $C_{\sigma|w}$ represent the concentration of the reactive agent in the fluid bulk and at the solid walls, respectively. L is the domain length and S_{total} is the total surface area of the pore structure with the unit of lu. ΔC_σ Represents the concentration difference of the reactive agent measured between the inlet to the outlet boundaries normalized by the minimum and maximum values of concentration (C_σ) within the domain. Upon how concentration boundary conditions are defined, the outlet concentration may be calculated by averaging all nodes at the outlet at different time steps during the simulations. Although, ΔC_σ may not be a constant, the normalized concentration is rather constant.

Convection-Diffusion equation may be also used to estimate the effective diffusion coefficient of a pore structure. That is the plot of left-hand side of Eq. (9) versus concentration Laplacian gives a slope equal to D_e , if the first and second order partial derivative terms are known.

$$\frac{\partial C}{\partial t} + \vec{u}_x \frac{\partial C}{\partial x} = D_{ex} \frac{\partial^2 C}{\partial x^2} \quad \text{Eq. (9)}$$

The concentration gradient and Laplacian may be calculated by the finite difference scheme using the 8 neighbour nodes at each site in the D2Q9 model (Huang et al., 2011):

$$\partial_\alpha C = \sum_{i=1}^{8} \frac{\omega_i \overrightarrow{e_{i\alpha}} C(x + \overrightarrow{e_{i\alpha}}\Delta t)}{c_s^2 \Delta t} \quad \text{Eq. (10)}$$

$$\partial_\alpha^2 C = 2\sum_{i=1}^{8} \frac{w_i (C(x + \overrightarrow{e_{i\alpha}}\Delta t) - C(x))}{c_s^2 (\Delta t)^2} \quad \text{Eq. (11)}$$

Since velocity, concentration and its first and second-order partial derivative terms are space-varying quantities, their values can be averaged over all pore nodes in the domain at different time steps during the simulations. On the other hand, as the literature suggests, a linear relation may exist between the effective diffusion in a pore structure and the Peclet number (Woods, 2015).

$$D_e / D_m = \alpha_{os} + \lambda Pe \quad \text{Eq. (12)}$$

where α_{os} and λ are constants that characterize the pore structure and D_m is molecular diffusion.

Dissolution at the solid boundary is a function of the reaction rate at the surface (Kang et al., 2014) such that:

$$\frac{\partial \varphi}{\partial t} = -V_m a_s \kappa (C - C_s) \quad \text{Eq. (13)}$$

In Eq. (13) V_m is the solid phase molar volume (i.e., the reactive mineral) κ is the average reaction rate constant with first order kinetics and a_s represents the specific surface area. The solid volume fraction φ will change at each time using Eq. (13) implemented at the interface nodes. When φ reaches zero, the corresponding node will turn into a fluid node, and its new adjacent solid nodes will act as the interface nodes. At the same time, the flow field is updated to account for the changes due to pore structure.

The Kozeny-Carman equation relates the porosity φ and permeability K of a porous bed if it can be considered as a bundle of non-connecting tortuous tubes with diameter D_p.

$$K = \frac{\varphi^3 D_p^2}{180(1-\varphi)^2} \quad \text{Eq. (14)}$$

But in reactive flow conditions, where the pore structure is modified by dissolution, the specific surface area is constantly changing. Therefore, permeability is needed to be correlated with a higher power of porosity. By rearrangement of Kozeny-Carman equation, a linear form can be derived in terms of $\sqrt{K/\varphi}$ and $\varphi_z = \varphi/(1-\varphi)$:

$$\sqrt{K/\varphi} = \sqrt{\frac{D_p^2}{180}}\left(\frac{\varphi}{1-\varphi}\right) = b.\varphi_z \quad \text{Eq. (15)}$$

In this form, we can investigate the deviation of porosity-permeability relation from the linear Eq. (15) due to the modification of the pore structure by dissolution in reactive flow condition. The permeability of the flow geometry can be evaluated from the velocity field using the Darcy law.

3. LBM on quadtree

The drawback to the conventional LB method is the use of spatially uniform lattice which cause excess computational load particularly when high resolution grid is required next to the solid boundaries. Here, we implemented a Quadtree grid refinement method to achieve higher resolution near the solid boundaries where detail information of concentration gradients become available to improve the simulation accuracy. In the next sections, we will discuss the considerable improvement of the computational efficiency using this method. The Quadtree scheme for domain decomposition usually utilizes a scale index (β) and a threshold (α) to control the grid density. While α is a constant, the scale

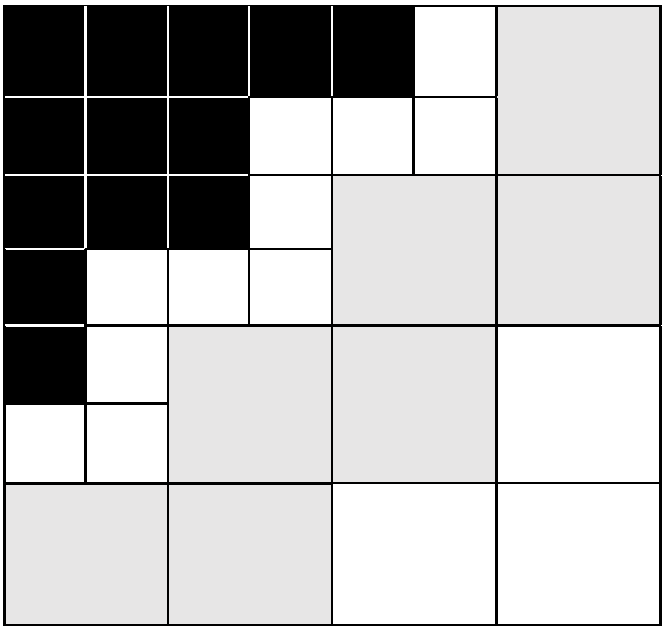

Fig. 2. The state of interface grids in Quadtree decomposition. The shaded colour shows the interface grids, each of which break into four fine grids in post-collision state.

index (β) indicates the fraction of solid-phase pixels (shown using black colours in different figures in this study) of a cell. Initially, we begin with one large square grid which is assigned to the entire domain (if we assume that the image to be reconstructed is a square). In the next step, the number of black pixels is divided by the number of all pixels within the square grid (i.e., the scale index β). Next, α, as a threshold parameter, is used to control the domain reconstruction, following these three main criterions: i) for $\beta > \alpha$, the grid value is set to one (i.e. black cells), ii) for $\beta < (1-\alpha)$, the grid value is set to zero (i.e., white cells), and iii) for cells for which the first two criterions is not valid, the grid is divided into four cells, each of which represents a new element. Discretization will be repeated for these new grids until the initial image is reconstructed. In this study, for all domain decompositions we have used a value of 1.0 for α to ensure that all curved boundaries will be reconstructed completely and without any modification to the primary porosity.

Next, the Lattice Boltzmann algorithm on cell-centred Quadtree is constructed by the following procedure (Chen et al., 2006):

- The collision-streaming calculations on the coarse grid at any time step have their corresponding two time-step calculation on the fine grids.
- For the interface grids, where a coarse grid is adjacent to a fine grid, a transfer function is implemented across the two grids. The interface belongs originally to the coarse grid, and, later, in the post collision state, the interface grids turn into components belonging to the fine grids. Fig. 2 shows such interface grids using a shaded colour.
- The interface grids, in post-collision state, break into four fine grids. Subsequently, the distribution data of the coarse interface grid (which are called parent grids) are associated with the fine grids (which are called child grids). This simply means that the four fine grids will have the same f and g values as the corresponding course grid.
- In the next stage, the streaming step is performed on the fine and children grids of the interface.
- The collision-streaming process is performed for the second time in the fine grid and the distribution data at the parent interface grids is recovered by averaging the distribution data of the children grids at the location of the interfaces.
- The final stage is the streaming step implemented at the coarse grid to reach the pre-collision state

In adaption of LBM on Quadtree grids the following criterions are needed to be considered:

- Both fine and coarse lattices should operate using the same speed (i.e., speed of sound which in D2Q9 is equal to). For a domain with two lattice sizes, the velocity term $c = \Delta x/\Delta t$, provide the corresponding time step which is $\Delta t_c = n\Delta t_f$, where n is the ratio of the coarse to fine grid size.
- Both fine and coarse lattices should provide the same viscosity. This criterion requires rescaling of the relaxation time for fine and coarse grids as $\tau_f = \left(\tau_c - \frac{\Delta t_c}{2}\right) + \frac{\Delta t_f}{2}$, with τ_c and τ_f being relaxation times of coarse and fine grids, respectively.
- The same density should be resulted from both lattices. As density and velocity are the same in fine and coarse grids, the force term should be modified to account for the grid type. This leads the gravity to be $g_f = g_c/n$ where n is the size ratio between coarse and fine grids.

Fig. 3 illustrates the change of distributions in the interface cells for the volumetric algorithm by Chen et al., (2006).

Fig. 4 shows two discretised porous media domains with 2 and 3 mesh sizes obtained using Quadtree method. For the case with more than 2 grid sizes (i.e., the 3 mesh quadtree) to simplify the calculations

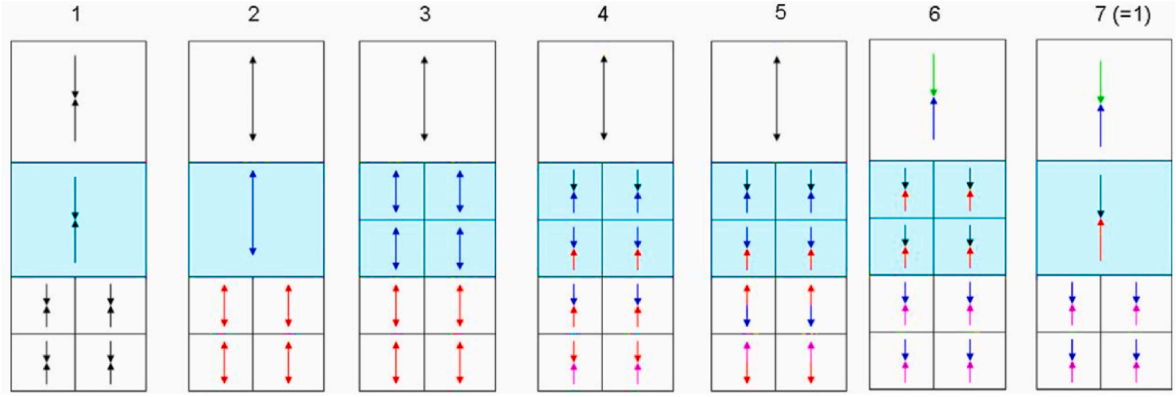

Fig. 3. Schematic of the change of distributions in the interface cells for the volumetric algorithm by Chen et al., (2006). A pair of distributions are shown. The "pre-collision" distributions are the arrows pointing toward the cell centre while the "post-collision" distributions are the arrows pointing away from the cell centre. Therefore, No. 2: collision in fine and coarse cells. No. 3: the breaking of the interface cell into 4 cells. No. 4: streaming in fine cells. No. 5: collision in inner fine cells and no. 6: streaming in fine and coarse cells to end up to state 7 (or 1) by recovering the coarse interface.

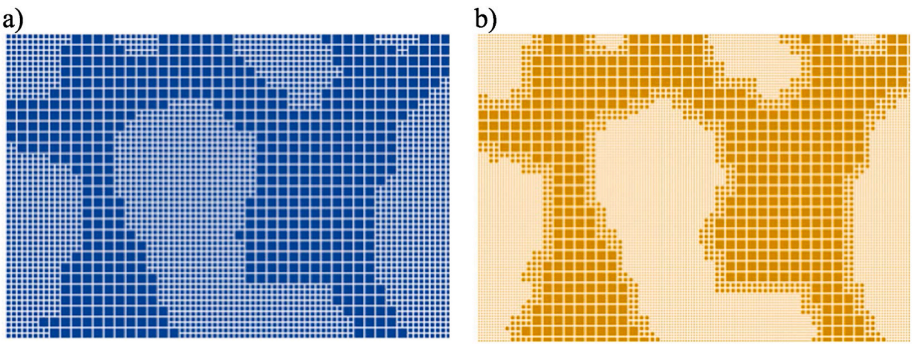

Fig. 4. a) 2-mesh Quadtree and b) 3-mesh Quadtree discretised porous media domains.

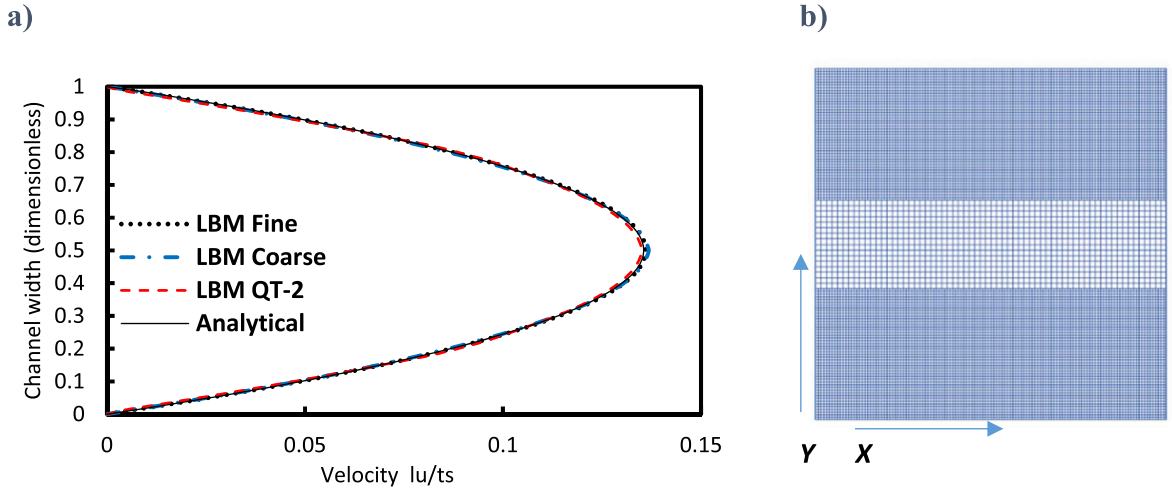

Fig. 5. a) fluid flow velocity profiles of flow calculated by different methods. The solid line indicates the analytical solution; the dotted line shows the fine-grid LBM and the dashed line (QT-2) corresponds to one-level refinement (or 2-mesh) Quadtree LBM results. **b)** 2-mesh Quadtree lattice of the channel where grid sizes are fine close to the top and bottom channel walls (with a dimension of 48 × 128 grids) and coarser grids are located in the middle of the channel (far from walls) with a dimension of 16 × 64.

at the grid interface, and to provide a smooth transition of the macroscopic variables across interfaces with different grid levels, only one size change between coarse cells and their fine neighbours is permitted (Fig. 4, b).

This criterion is implemented by adding an extra step to the domain decomposition algorithm. In this step, we seek for any large size cells with unsuitable difference level, which have sides or corners located at the boundaries of the fine grid, and we divide each of them into four new elements.

4. Model validation

In this section, we start validating the developed Quadtree scheme against a benchmark problem for which analytical solutions exist together with results obtained using the conventional LBM. Next, we tackle a series of progressively complex flow and transport simulations including fluid flow, tracer transport, and reactive transport in single pores, and reactive transport in dissolving porous media.

4.1. Fluid flow in a 2D channel

At the first validation step, we use the developed Quadtree scheme to simulate flow in a 2D channel which can be described using Poiseuille formula. The fine grid model operates on a domain size of 128 × 128 grids, and hence the coarse grid size is 64 × 64 grids. In the 2-mesh Quadtree model, the grid sizes are fine close to the channel walls with a dimension of 48 × 128 grids. The coarser grids are located within the channel bulk space and have a dimension of 16 × 64 grids. This simulation implemented periodic and bounce back boundaries at the inlet/outlet and the top/bottom walls, respectively. With the Guo et al., (2002) scheme, the applied body force is 4×10^{-5} mu/(lu.ts^2). Under the same flow conditions, the fine and coarse grid models are compared with the quadtree results as well as the analytical solution.

Fig. 5 shows an excellent agreement between LBM results and the analytical solution based on Poiseuille formula. The error analysis of the calculated velocity profile regarding the analytical solution of the flow is provided in Table 1. Comparison of different lattice types clearly shows that the Quadtree model is able to reproduce the analytically obtained velocity profile with high accuracy. The simulation based on 2-mesh Quadtree resulted in an error less than 1.0% relative to the analytical solution which indicates that quadtree model has a precision between the fine- and the coarse-grid models.

Table 1
Error analysis of the velocity profile of flow calculated by different lattice type for Poiseuille flow.

Lattice type	Ave relative error	$RRMSE = \sqrt{1/n \sum (u_i - \hat{u})^2/(\hat{u})^2}$
2- mesh Quadtree	0.004	0.0093
Fine grid	0.002	0.0054
Coarse grid	0.008	0.0165

* RRMSE indicates the Relative Root-Mean-Squared Error with respect to the analytical solution.

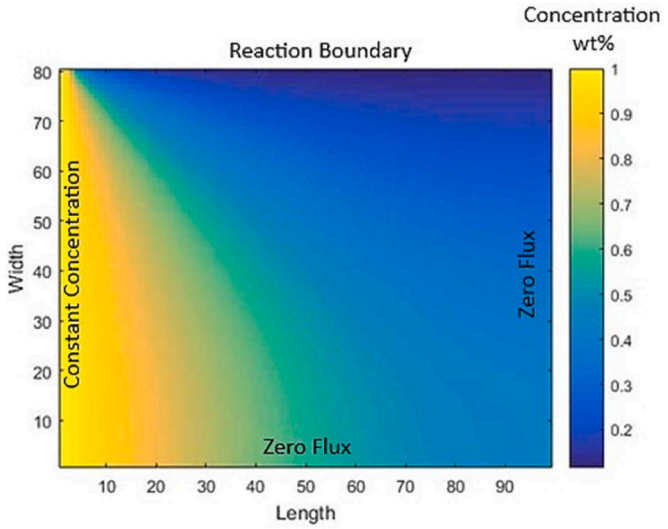

Fig. 6. Boundary conditions and the typical result by Quadtree method.

4.2. Diffusive reactive transport in a 2D channel

For this section, we use the example reported by Kang et al., (2007) to simulate a diffusive-reactive problem. The simulation domain is a rectangular pore in which reaction takes place at the top boundary. The right and bottom boundaries are at zero flux condition. A constant concentration is considered at the left boundary which diffuses into the domain during the simulation. Such a diffusive reactive problem can be presented by Laplace's equation.

$$\frac{\partial^2 C}{\partial x^2}+\frac{\partial^2 C}{\partial y^2}=0 \qquad \text{Eq. (16)}$$

Initially, the occupying fluid solution in the domain is not reacting with the solid phase. Upon beginning of the simulation, the concentration value at the left boundary is set to $C_0 = 1.0$ which begins to diffuse into the domain and react with the solid phase located at the top boundary. The simulation domain for the uniform fine grid model is equal to 80 × 100 grids. In the Quadtree model, the grids adjacent to the reacting wall are fine, providing a dimension of 14 × 100 grids. The coarse section of the domain has a dimension of 33 × 50 grids. The uniform coarse grid model has a dimension equal to 40 × 50 grids. Similar to other studies (Kang et al., 2014; Mostaghimi et al., 2016; Yoon et al., 2015; Machado, 2012), we use the relative influence of reaction over diffusion to be the same as the value used by Kang et al., (2007) i.e., the Damköhler number, $Da = \kappa L/D_m = 48$ where L is the characteristic length corresponds to the left side of the domain, $D_m = 0.16$ lu^2/ts and $\kappa = 0.1$ lu/ts.

Fig. 6 demonstrates the boundary conditions that were applied to the model and shows typical simulation result. The analytical solution and the calculated concentration profile by quadtree model are shown in Fig. 7.

Table 2 provides the analysis of the simulation. We should note that the spatial distribution of a specific concentration $C = 0.5$ was used to evaluate the error. Fig. 7 and Table 2 show that the Quadtree model successfully generated the correct concentration profile and provided results very close to that of analytical solution.

4.3. Advective-diffusion reactive transport in a single pore

In this section, we use the verification problem used by Kang et al., (2007) who applied the thermal-hydrologic-chemical Finite Difference model, PFLOTRAN, developed by Lichtner (1999) for model verification. In this test, a prescribed Poiseuille velocity profile is established in a single pore with a Peclet number $Pe = UL/D_m = 12$, where L is the characteristic height of the domain, $D_m = 0.16$ lu2/ts and U is the average fluid velocity. The simulation size for the uniform fine grid model, is 60 × 400 grids. In the Quadtree model, the grids are finer near the reacting surfaces providing a dimension of 6 × 400 grids and the coarse middle part of the domain has a dimension of 24 × 200 grids. For the uniform coarse grid model, the dimensions equal to 30 × 200 grids.

Table 2
Error analysis of the spatial concentration distribution calculated by different lattice types for the diffusive-reactive transport in a rectangular pore.

Lattice type	Ave relative error	$RRMSE = \sqrt{1/n\sum (y_i-\hat{y})^2/(\hat{y})^2}$
2-mesh Quadtree	0.12	0.18
Fine grid	0.09	0.13
Coarse grid	0.16	0.21

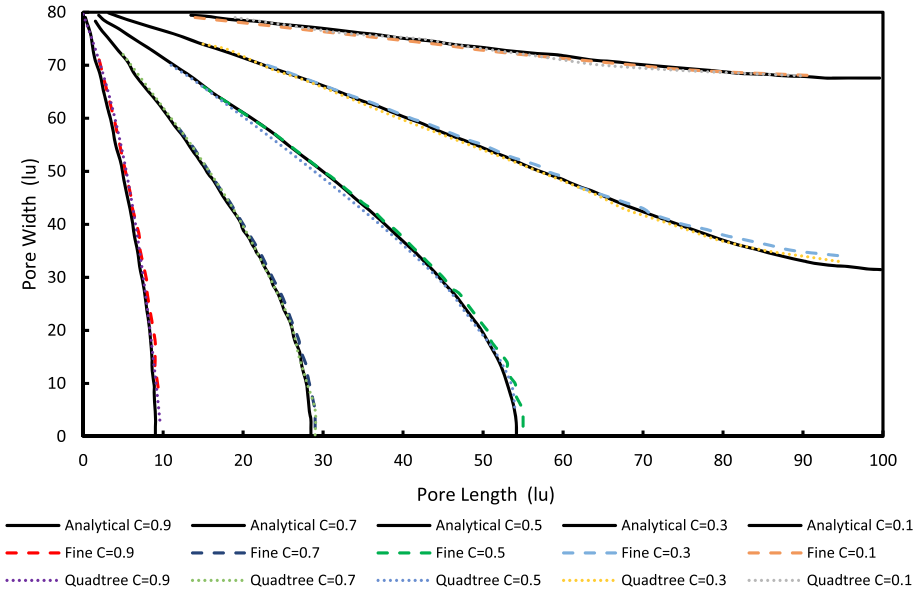

Fig. 7. Concentration profile for a diffusive-reactive simulation carried out in a rectangular domain of size 80 × 100 grids. The lines show the analytical solution of the laplace equation.

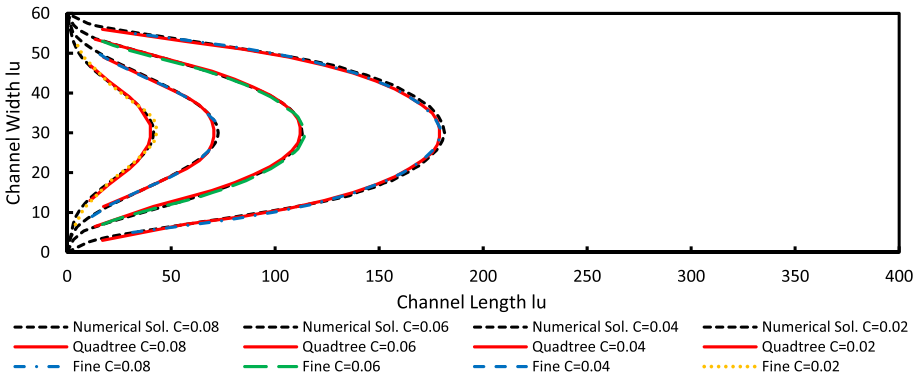

Fig. 8. Concentration profile for Convection, Diffusion and Reaction in an open channel with $Da = 75$. The lines represent the numerical solution of PFLOTRAN generated by Kang et al., (2007).

Table 3
Error analysis of the spatial concentration distribution calculated by different lattice types for the advective-diffusion-reactive transport in a single pore. The unit of the error is lattice unit.

Lattice type	Ave relative error	$RRMSE = \sqrt{1/n \sum (y_i - \hat{y})^2/(\hat{y})^2}$
2-mesh quadtree	0.05	0.12
Fine grid	0.03	0.09
Coarse grid	0.08	0.15

The top and bottom boundaries act as no-flow boundaries. Initially, the fluid is not reacting with the solid walls ($C_s = 0.1$). At the start of simulation, a solution with a concentration of $C = 1 \times 10^{-8}$ is injected from the left boundary and reaction takes place at the walls. The outlet is maintained at a zero-concentration gradient.

Fig. 8 shows the established concentration profiles, calculated by fine grid and Quadtree LBM models for the flow with $Da = \kappa L/D_m = 75$ where $\kappa = 0.2$ lu/ts. Table 3 provides the error associated with different lattice types by considering the spatial distribution of a specific concentration $C = 0.08$. The results show a very good agreement with the numerical concentration profile reported by Kang et al., (2007).

5. Results and discussions

In this section, we use the developed Quadtree model to simulate reactive transport in a porous media in form of solid phase dissolution. We characterize the porous media using dimensionless parameters including Reynolds, Peclet, Damköhler, and Sherwood numbers. We will discuss the effectiveness and accuracy of the Quadtree simulations with different resolutions using both uniform and Quadtree LBM.

5.1. Time efficiency of the quadtree method

In order to investigate the efficiency of the computational time quantitatively, a reactive transport model for a pore scale channel with the reactions taking place at the solid walls is considered. In this simulation, no dissolution of the solid phase is taken into account. In the next case, a more complex, porous structure, domain is selected where similar boundary conditions are applied including constant velocity/pressure boundary at the inlet/outlet, respectively, together with the periodic boundary conditions at the top and bottom boundaries. The standard bounce-back method is applied at the solid surfaces. For solute transport, constant concentration is applied at the inlet, and zero diffusive flux is applied at the outlet boundary. The computer codes for Quadtree mesh generation and flow simulation were developed using

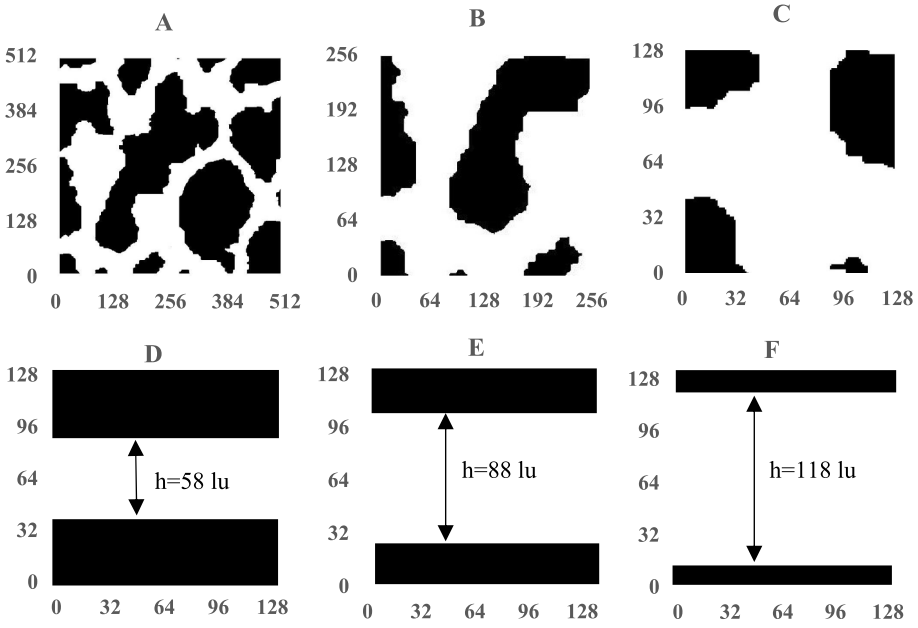

Fig. 9. Different pore structures for comparison of the simulation time using Quadtree method.

Table 4
Computational time required to perform 1000 time steps using the fine grid and the Quadtree model with one and two-level refinement (2-mesh and 3-mesh lattice types respectively). The pore structures A-to-F are shown in Fig. 9.

Pore Structure	Dimension	Porosity	Fine grid time	2-mesh Quadtree	Fine/Coarse grids	Qt-2/fine time ratio	3-mesh Quadtree	Fine/Coarse grids	Qt-3/fine time ratio
A	512 × 512	54%	2689 s	1155 s	1	0.43	1075 s	4	0.40
B	256 × 256	63%	790 s	317 s	0.84	0.40	275 s	3.2	0.35
C	128 × 128	73%	212 s	98 s	1	0.46	84 s	4	0.40
D	128 × 128	45%	131 s	54 s	0.83	0.41	60 s	4	0.46
E		68%	198 s	65 s	0.4	0.33	55 s	1.78	0.28
F		92%	274 s	82 s	0.37	0.30	52 s	0.92	0.19

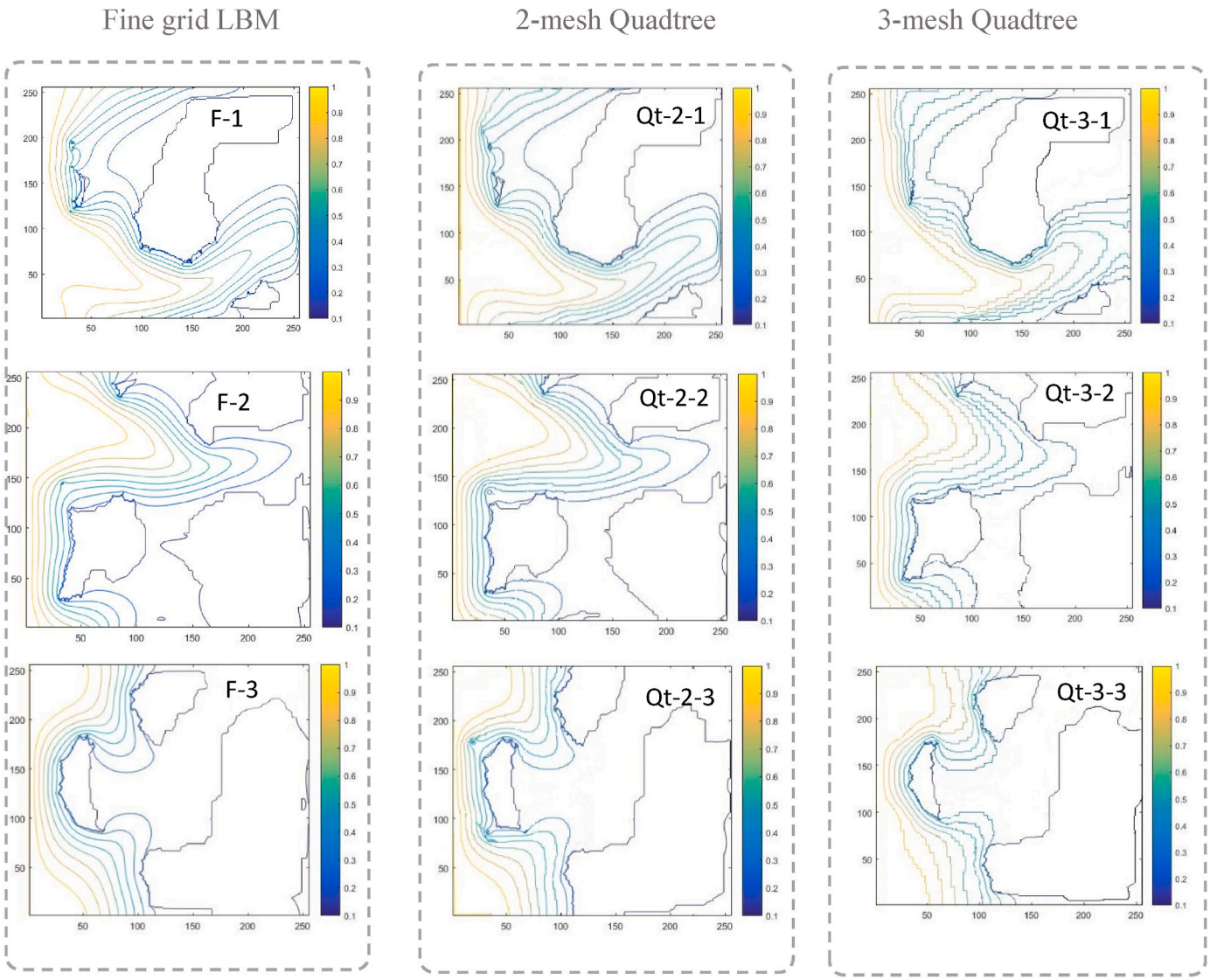

Fig. 10. Reactive transport in porous media. The first column shows the concentration contours obtained using the fine grid LBM; the second column shows similar results using the 2-mesh Quadtree model; the third column shows results using the 3-mesh Quadtree method. The fields show concentration distributions of the reactive agent after 5000 time steps in simulation, using a solution with $Da = 100$. The colour bar demonstrates the concentration distribution from 0 to 1.

the MATLAB software and simulated with an intel core i7-740QM 2.5 GHz processor with 4 GB DDR3 1333 MHz RAM.

Fig. 9 shows the applied simulation pore structures and Table 4 provides the computational times required to perform 1000 time steps.

In Table 4, the column "Fine/Coarse grids" indicates the ratio of the number of fine grids to the number of coarse grids within the pore space. For the pore structure "A" this ratio is equal to 1 when it is decomposed by a 2-mesh Quadtree lattice (or Qt-2) and equal to 4 if 3-mesh Quadtree (or Qt-3) is implemented. The difference in Qt-3 is due to the number of larger grids which makes the denominator of this ratio to be smaller. In general, it is expected that as the number of coarse grids approaches those of fine grids or becomes greater, the computational time will decrease.

Table 4 shows the clear computational advantages of applying Quadtree mesh refinement. The results show that the Qt-2 is computationally more efficient compared to simulations using the fine grid. The level of acquired efficiency depends on the pore structure where the Qt-2 showed up to three times speedup compared to LBM simulations using a

Table 5
Comparison of dissolution of porous media for different pore structures and at different Damköhler numbers.

Lattice type-pore structure	Porosity	fraction of solid interface nodes	fraction of dissolved solid phase (Da = 20)	fraction of dissolved solid phase (Da = 100)
F- 1	0.66	0.136	0.139	0.278
Qt-2 - 1			0.152	0.275
Qt-3 - 1			0.136	0.274
F- 2	0.58	0.108	0.080	0.139
Qt-2 - 2			0.084	0.153
Qt-3 - 2			0.080	0.151
F-3	0.55	0.124	0.121	0.212
Qt-2 - 3			0.122	0.206
Qt-3 - 3			0.119	0.238

uniform grid. When using the Qt-3, we have obtained up to five times speedup relative to using a regular fine grid, which indicates a major improvement in the computational efficiency. For the case of porous media structures, i.e., structures A and B, Table 4 implies that for larger domain sizes the time efficiency becomes more significant as the fine grid model took 2700 s to complete while Qt-3 consumed about 1000 s. In case of porous media structure with low porosity values, higher resolution images of the porous media are required for which the Qt-3 becomes more efficient relative to the 2-mesh Quadtree method.

5.2. Dissolution reactions in porous media using the quadtree method

In order to simulate a complex problem where both reaction and dissolution are simultaneously occurring, we apply a complex porous media structure with curved boundaries. The Quadtree decomposition used in this study is not dynamic and adaptive over time. Therefore, as chemical dissolution proceeds, the simulation continues with the initial domain decomposition. Here we select different parts of the pore structure A in Fig. 9 with the sample dimensions equal to 256 × 256 grids to compare the quadtree performance on different lattices but in the next section, we will implement large simulation dimensions to achieve representative results. The flow and concentration boundary conditions are the same as previous section but the dissolution is now active and considered to modify the pore structure. Reaction and zero flux boundaries are applied at the solid surfaces. The results for both uniform and Quadtree LBM with 2 and 3 mesh sizes are presented in Fig. 10 and Table 5.

For comparison between different numerical schemes, three cases are provided in Fig. 10: i) fine uniform lattice (F-X), ii) 2-mesh Quadtree (Qt-2-X), and iii) 3-mesh Quadtree (Qt-3-X) lattices. The results show similar behaviours among different models, however, there is a slight difference between models for the dissolved solid phases. The visualization of concentration distributions (according to the shown concentration colour bar) in Fig. 10 are also affected by model resolutions (e.g., between Quadtree and coarse-grid models) because different models apply different grid sizes. We consider the results obtained using the fine-grid LBM as the most numerically accurate results. Quantitative simulation results are provided in Table 5 which verify the consistency of Quadtree models. Table 5 reports the amount of reactive solid surfaces and the corresponding fraction of dissolved solid phases for two different Damköhler numbers of $Da = 20$ and $Da = 100$. The fraction of solid interface nodes (which affect dissolution and the reaction rate) is determined by the ratio of total solid interface nodes to all solid nodes. The fraction of dissolved solid can be simply obtained by subtracting the final porosity from initial porosity. Table 5 also compares the results of fine-grid LBM with Quadtree method for each structure. It is clear that the Quadtree could successfully predict the dissolution of the structures in agreement with fine-grid LBM.

Furthermore, as we remember the Poiseuille reactive flow in a single pore in Fig. 8, it is clear that the concentration distribution is highly affected by the flow velocity field. However, while the concentration profiles illustrate dependency on the local velocity, the velocity depends on the flow path in fluid flow through porous media. Fig. 11 compares the velocity profiles for Qt-2 and Qt-3 models in pore structure 1 of Fig. 10 and outlines the flow path effect on the velocity. The colour bar demonstrates the velocity distribution from 0 to 0.12 lu/ts. Therefore, the similar concentration profiles in each pore structure in Fig. 10 imply the presence of a similar velocity field.

5.3. Investigation of mass transfer coefficients

Here we consider two pore structures shown in Fig. 12 to investigate the variation of Sherwood number. The simulation parameters and their dimensional analysis are summarized in Table 6. The value of $C_{\sigma|b}$ at the inlet is set to 0.1 and $C_{\sigma|w}$ which represents the concentration at the solid walls will be the minimum value at the outlet. The boundary conditions are constant concentration at inlet and zero concentration gradient at outlet. In this simulation, the rate of dissolution is slow ($Da = 0.1$) and the pore structure is almost constant.

Eq. (8) suggests that the log-scale plot of $ShSc^{-1/3}$ versus Re provides a linear relation. This linear relation can be used as a measure of the model robustness, as the experimental data in Yoshino and Inamuro (2003) approve the linear correlation of Sherwood and Reynolds numbers.

Fig. 13 compares the calculated results obtained from fine-grid LBM (which is considered the accurate response) and the 2-mesh Quadtree model for different simulation cases. The results show that the Quadtree

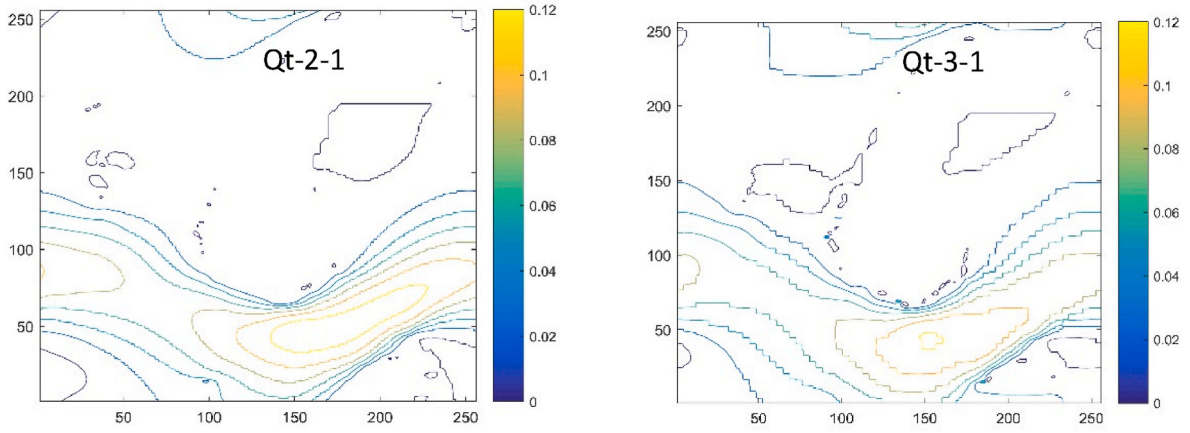

Fig. 11. Comparison of the velocity field for Qt-2 and Qt-3 models in pore structure 1. The colour bar demonstrates the velocity distribution from 0 to 0.12.

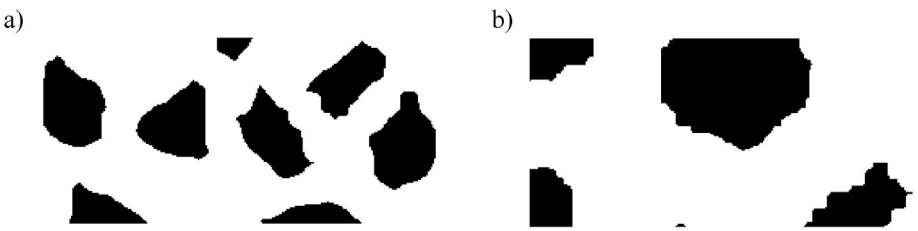

Fig. 12. The two flow geometry structures used for investigation of the mass transfer coefficient. The dimension of the flow domain is 128 × 256.

Table 6
Dimensional analysis of LBM parameters for modelling simultaneous reaction and dissolution.

Parameters	Physical system		LBM		Conversion factor
Length	1	[cm]	128	lu	$C_L = L_{real}/L_{LB}$
Kinematic viscosity	0.01	[cm^2/s]	0.35	lu^2/ts	$C_\upsilon = \upsilon_{real}/\upsilon_{LB}$
Flow velocity	0.1	[cm/s]	0.027	lu/ts	$C_u = C_\upsilon/C_L$
Time	1	[Sec.]	500	ts	$C_t = {C_L}^2/C_\upsilon$
Reaction constant	0.01	[cm/s]	0.0027	lu/ts	$C_r = C_u$
Diffusivity	0.003	[cm^2/s]	0.105	lu^2/ts	$C_{dif} = D_{real}/D_{LB}$
Concentration	1	wt%	1	wt%	–
Specific surface area	44	[cm^2/cm^3]	0.34	lu/lu^2	$C_a = 1/C_L$
Density	1	[g/cc]	1	mu/lu^2	$C_\rho = \rho_{real}/\rho_{LB}$

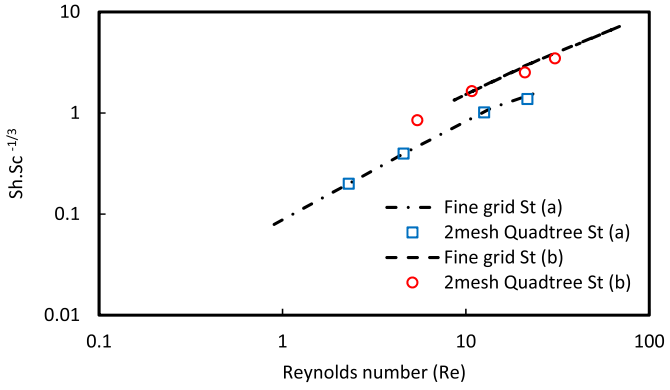

Fig. 13. Comparison of computed $ShSc^{-1/3}$ versus *Re* in a domain of size 128 × 256 for fine-grid LBM and 2-mesh Quadtree model. In this simulation, no dissolution of the solid phase is taken into account. The consistent linear relation that is obtained for different pore structures (a) and (b) in Fig. 12, demonstrates the quadtree model robustness.

model is consistent with the calculated Sherwood number by the fine grid model under different Reynolds numbers. Moreover, as Fig. 13 suggests, in addition to the Reynolds number which emphasizes the role of advection in mass transfer, the change in the pore structure may affect the mass transfer coefficient considerably. The pore structure shown in Fig. 12b has coarser grains and higher permeability which results in larger Sherwood. The consistent linear relation that is obtained for the different structures (a) and (b) in Fig. 12, demonstrates the quadtree model robustness.

Fig. 14 plots the effective diffusion coefficient (dispersion) against the Peclet number obtained by the Quadtree model for the pore structure in Fig. 12a. This plot measures the model's ability in demonstrating the expected macro-scale behaviour defined by Eq. (12). The results show that the Quadtree model is clearly producing a linear relation that can be used to obtain the parameters α and λ of the pore structure.

The quadtree model is then implemented to investigate the alteration

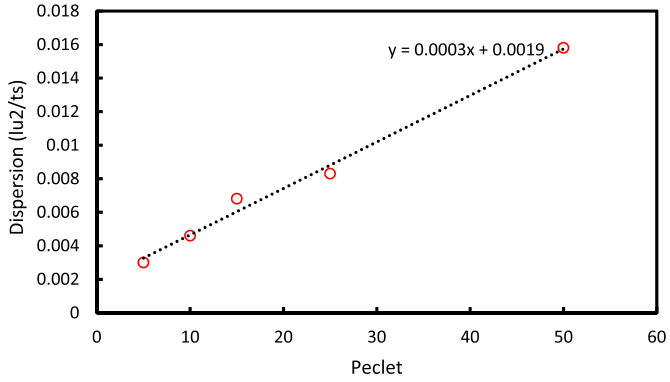

Fig. 14. Computed dispersion coefficient at different Peclet numbers for the pore structure in Fig. 12a by Quadtree model. In this simulation, no dissolution of the solid phase is taken into account.

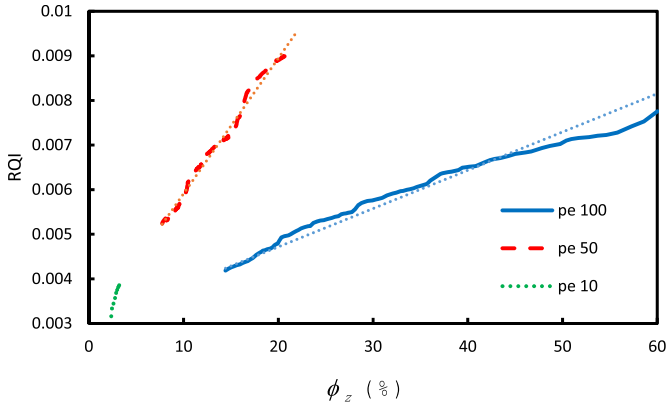

Fig. 15. Comparison of the computed variation in RQI versus φ_z at different Peclet numbers at $Da = 400$. The simulation conducted for 40,000 time steps.

of porosity-permeability relation by the reactive flow. The pore structure in Fig. 12a is implemented with the dimension of 512 × 1024 grids. Furthermore, $Da = 400$ and Peclet numbers of 10, 50 and 100 are considered. This range of Peclet produces three different dissolution patterns: $Pe = 10$ yields face dissolution, $Pe = 50$ creates wormhole and $Pe = 100$ results in ramified or uniform dissolution. In the latter two cases, the alteration of porosity-permeability is considerably high while in the first case with low Peclet flow, the pore structure experiences a minimum modification. Fig. 15 plots $RQI = \sqrt{K/\varphi}$ versus $\varphi_z = \varphi/(1-\varphi)$ during 40,000-time steps of the simulation. The values of RQI (Rock Quality Index) and φ_z were calculated at different time steps during the simulation. The results show that higher flow rates by forcing more acid into the pore structure can cause a major difference in the porosity-permeability relation where the deviation from the linear trend implies deviation from the Kozeny-Carman equation. While $Pe = 50$ shows more increase in RQI, a major increase of φ_z occurred in case of $Pe = 100$, and both cases show deviation from linearity. In case of $Pe = 100$

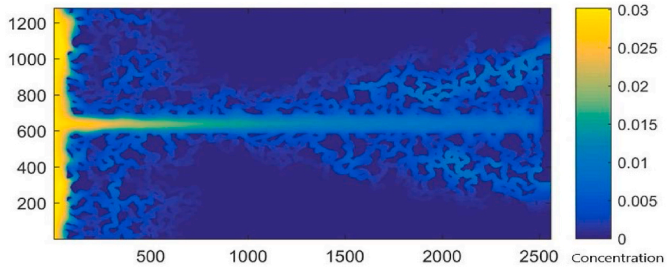

Fig. 16. The developed flow in a closed-end fracture with porous walls, size 1280 × 2560 grids at $Da = 50$ and $Pe = 50$ after 40,000 time steps.

or ramified dissolution, the pore structure undergoes severe dissolution as the change of φ_z from 15 to 60 percent highlights it.

These examples of quadtree application clearly prove the capability of quadtree grid refinement in reactive flow simulation. The interesting outcome is the macroscopic properties that can be scaled up from the pore structure directly. In the following we apply the developed model to a closed-end fracture with porous walls to evaluate the dispersion and Sherwood. A large domain size of 1280 × 2560 grids is chosen to have sufficiently up-scaled and average properties extracted. We also consider slow rate of dissolution to have minimum modification of the pore structure and obtain state dependent properties, i.e., $Da = 50$ and $Pe = 50$ with the inlet concentration equal to 0.03. Fig. 16 shows the developed flow in the fracture after 40,000 time steps.

According to Eq. (9) the effective diffusion coefficient equals to the slope of the plot of the left-hand side (sum of the concentration difference per time step and product of velocity and concentration gradient) versus concentration Laplacian. As we mentioned earlier, velocity, concentration and its partial derivatives are averaged over all pore nodes in the domain at different time steps during the simulations. The result plot in Fig. 17 interestingly shows three distinct values illustrated with three different colours. At the early flow time, when the flow intrudes the fracture, the dispersion is large due to the high advection effect. At mid time, when the pressure gradient the fracture's tip imposes flow into porous walls, a decrease in dispersion occurred due to the tortuosity effect. And ultimately at the late time the net fracture-porous walls act as a unified medium with lower value for effective diffusion coefficient.

The prescribed three flow behaviours also affect the Sherwood number as Fig. 18 clearly shows the initial, transitional and the final effect due to the different flow conditions imposed in the medium.

Therefore, the great point of Quadtree models is the ability to study the pore scale mechanisms with the acquired efficiency and a step forward to perform large-size pore scale simulation. This step is needed to incorporate the effect of the underlying micro-scale processes into continuum scale simulations of porous media dissolution.

6. Conclusions

In this study, we have developed a Quadtree model decomposition to increase the computational efficiency of the lattice Boltzmann model in simulating fluid flow and reactive transport at the pore scale. The developed method was verified against several benchmark problems with different levels of complexity. The accuracy and the computational benefits of the developed scheme were discussed in detail by comparing the Quadtree model against fine-grid LBM and coarse-grid LBM simulations. As main conclusions:

- The Quadtree model reconstructs the bulk pore spaces using coarse grids where high resolution is maintained adjacent to the solid phases by applying local fine-grid mesh. The Quadtree model uses a cell-centred approach based on the scheme developed by Chen et al., (2006) which is mass conservative and simple to be applied since it requires no interpolation or change in non-equilibrium density distribution function to acquire second order accuracy. We have applied a D2Q9 LB model, for both flow and solute transport, with additional

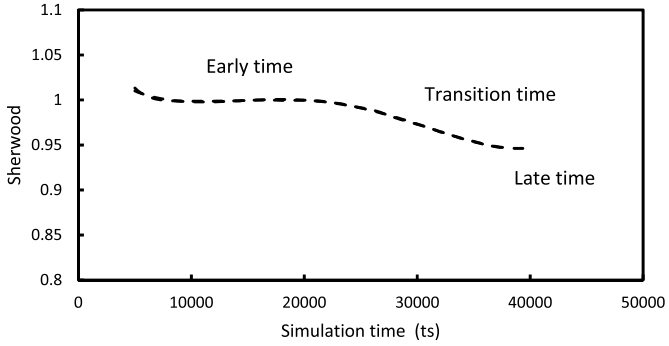

Fig. 18. Comparison of different Sherwood values during flow through a closed-end fracture with porous walls. The net flow at the late time, shows lower Sherwood.

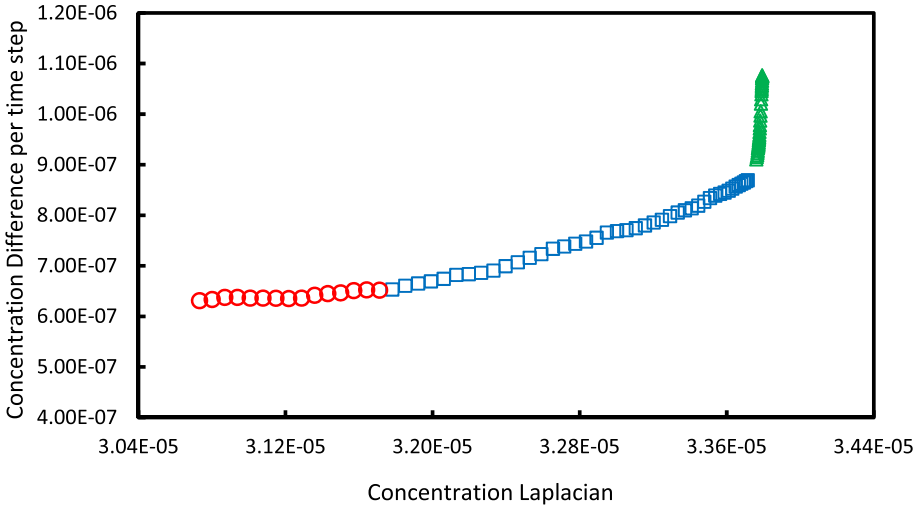

Fig. 17. Comparison of different dispersion effects during flow through a closed-end fracture with porous walls. Green indicates early time advection, blue shows the transition from fracture advection to porous medium flow, and red correspond to the net flow in fracture-porous walls.

terms applied at the nodes neighbouring the solid phases to simulate reactive transport.

- In order to validate the Quadtree method, several flow and transport problems were simulated including Poiseuille flow in a 2D channel, reactive-diffusive transport in a rectangular domain, and advective-diffusive-reactive flow and transport in a 2D channel. While the first case provides analytical solutions to verify the numerical scheme, the latter two cases are used by Kang et al., (2007) to validate their reactive LBM model. For each simulation, the results from both fine-grid LBM and Quadtree method were presented and discussed in terms of their accuracy and computational benefits. The results have shown major improvements in computational time while the accuracy of the model remained high and close to that of fine LBM which took much longer to perform the simulations under similar conditions.
- For reactive transport, the 3-mesh Quadtree method could provide up to five times simulation speedup depending on the porous media structure. Also, the 3-mesh Quadtree method provided more efficiency for simulations using high resolution digital images. The 2-mesh Quadtree method showed to be up to three times faster than the regular technique. Finally, we have shown the efficiency of the Quadtree method to simulate reactive transport with dissolution of the solid phases and change of pore structures. The results were further used to estimate porous media macroscopic properties using average mass transfer coefficients which can be used for upscaling from pore scale to the continuum scale.
- The Quadtree model was applied to two different large-scale domains to investigate the porosity-permeability deviation from Kozeny-Carman relation during dissolution at different Peclet numbers and moreover, to study the average mass transfer coefficients in a fractured porous media during reactive flow. The simulation results clearly highlight the Quadtree ability to study the pore scale mechanisms in reactive flow through porous media.

Credit author statement

Sadegh Mahmoudi: Methodology, Software, Validation, Formal Analysis, Investigation, Data Curation, Writing – Original Draft, Writing – Review & Editing, Visualization., Shahab Ayatollahi: Supervisor, Conceptualization, Review & Editing, Saeid Jamshidi: Supervisor, Conceptualization, Review & Editing, Amir Raoof: Advisor, Conceptualization, Review & Editing, Sharif University of Technology: Project administration.

Declaration of competing interest

The authors declare that they have no known competing financial interests or personal relationships that could have appeared to influence the work reported in this paper.

Appendix A. Supplementary data

Supplementary data to this article can be found online at https://doi.org/10.1016/j.jngse.2022.104674.

References

Chen, H., Filippova, O., Hoch, J., Molvig, K., Shock, R., Teixeira, C., Zhang, R., 2006. Grid refinement in lattice Boltzmann methods based on volumetric formulation. Phys. Stat. Mech. Appl. 362 (1), 158–167.

Chen, L., He, Y.-L., Kang, Q., Tao, W.-Q., 2013. Coupled numerical approach combining finite volume and lattice Boltzmann methods for multi-scale multi-physicochemical processes. J. Comput. Phys. 255, 83–105.

Chen, Y., Kang, Q., Cai, Q., Zhang, D., 2011. Lattice Boltzmann method on quadtree grids. Phys. Rev. 83 (2), 026707.

Crouse, B., Rank, E., Krafczyk, M., Tölke, J., 2003. A LB-based approach for adaptive flow simulations. Int. J. Mod. Phys. B 17, 109–112, 01n02.

Filippova, O., Hänel, D., 1998. Grid refinement for lattice-BGK models. J. Comput. Phys. 147 (1), 219–228.

Foroughi, S., Jamshidi, S., Masihi, M., 2013. Lattice Boltzmann method on quadtree grids for simulating fluid flow through porous media: a new automatic algorithm. Phys. Stat. Mech. Appl. 392 (20), 4772–4786.

Gao, J., Xing, H., Tian, Z., Pearce, J.K., Sedek, M., Golding, S.D., Rudolph, V., 2017. Reactive transport in porous media for CO2 sequestration: pore scale modeling using the lattice Boltzmann method. Comput. Geosci. 98, 9–20.

Guo, Z., Zheng, C., Shi, B., 2002. Discrete lattice effects on the forcing term in the lattice Boltzmann method. Phys. Rev. 65 (4), 046308.

Huang, H., Wang, L., Lu, X.-y., 2011. Evaluation of three lattice Boltzmann models for multiphase flows in porous media. Comput. Math. Appl. 61 (12), 3606–3617.

Jiang, M., Xu, Z., 2021. Pore-scale investigation on reactive flow in non-uniform dissolved porous media considering immiscible phase by lattice Boltzmann method. J. Nat. Gas Sci. Eng. 96, 104280.

Jiménez-Hornero, F.J., Giráldez, J., Laguna, A., 2004. Estimation of the role of obstacles in the downslope soil flow with a simple erosion model: the analytical solution and its approximation with the lattice Boltzmann model. Catena 57 (3), 261–275.

Kang, Q., Chen, L., Valocchi, A.J., Viswanathan, H.S., 2014. Pore-scale study of dissolution-induced changes in permeability and porosity of porous media. J. Hydrol. 517, 1049–1055.

Kang, Q., Lichtner, P.C., Zhang, D., 2007. An improved lattice Boltzmann model for multicomponent reactive transport in porous media at the pore scale. Water Resour. Res. 43 (12).

Kang, Q., Zhang, D., Chen, S., He, X., 2002. Lattice Boltzmann simulation of chemical dissolution in porous media. Phys. Rev. 65 (3), 036318.

Kermani, M.S., Jafari, S., Rahnama, M., Raoof, A., 2020. Direct pore scale numerical simulation of colloid transport and retention. Part I: fluid flow velocity, colloid size, and pore structure effects. Adv. Water Resour. 144, 103694.

Knutson, C.E., Werth, C.J., Valocchi, A.J., 2001. Pore-scale modeling of dissolution from variably distributed nonaqueous phase liquid blobs. Water Resour. Res. 37 (12), 2951–2963.

Krüger, T., Kusumaatmaja, H., Kuzmin, A., Shardt, O., Silva, G., Viggen, E.M., 2017. The lattice Boltzmann method. Springer Int. Publ. 10 (978–3), 4–15.

Li, L., Mei, R., Klausner, J.F., 2017. Lattice Boltzmann models for the convection-diffusion equation: D2Q5 vs D2Q9. Int. J. Heat Mass Tran. 108, 41–62.

Lichtner, P., 1999. Flotran Users Guide, report." Los Alamos Natl. Lab.. Los Alamos, NM.

Lichtner, P.C., Kang, Q., 2007. Upscaling pore-scale reactive transport equations using a multiscale continuum formulation. Water Resour. Res. 43 (12).

Liu, S., Zhang, C., Ghahfarokhi, R.B., 2021. A Review of lattice-Boltzmann models coupled with geochemical modeling applied for simulation of advanced waterflooding and enhanced oil recovery processes. Energy Fuels 35 (17), 13535–13549.

Machado, R., 2012. Numerical simulations of surface reaction in porous media with lattice Boltzmann. Chem. Eng. Sci. 69 (1), 628–643.

Min, T., Gao, Y., Chen, L., Kang, Q., Tao, W.-w., 2016. Changes in porosity, permeability and surface area during rock dissolution: effects of mineralogical heterogeneity. Int. J. Heat Mass Tran. 103, 900–913.

Montemore, M.M., Montessori, A., Succi, S., Barroo, C., Falcucci, G., Bell, D.C., Kaxiras, E., 2017. Effect of nanoscale flows on the surface structure of nanoporous catalysts. J. Chem. Phys. 146 (21), 214703.

Mostaghimi, P., Liu, M., Arns, C.H., 2016. Numerical simulation of reactive transport on micro-CT images. Math. Geosci. 48 (8), 963–983.

Parvan, A., Jafari, S., Rahnama, M., Raoof, A., 2020. Insight into particle retention and clogging in porous media; a pore scale study using lattice Boltzmann method. Adv. Water Resour. 138, 103530.

Patel, R.A., Perko, J., Jacques, D., De Schutter, G., Van Breugel, K., Ye, G., 2014. A versatile pore-scale multicomponent reactive transport approach based on lattice Boltzmann method: application to portlandite dissolution. Phys. Chem. Earth, Parts A/B/C 70, 127–137.

Ponce Dawson, S., Chen, S., Doolen, G.D., 1993. Lattice Boltzmann computations for reaction-diffusion equations. J. Chem. Phys. 98 (2), 1514–1523.

Soleimani, R., Norouzi, S., Rasaei, M.R., 2019. Investigation of gas condensate drop-out effect on gas relative permeability by Lattice Boltzmann modelling. Can. J. Chem. Eng. 97 (6), 1921–1930.

Succi, S., Amati, G., Bernaschi, M., Falcucci, G., Lauricella, M., Montessori, A., 2019. Towards exascale lattice Boltzmann computing. Comput. Fluid 181, 107–115.

Tong, Z.-X., He, Y.-L., 2015. A unified coupling scheme between lattice Boltzmann method and finite volume method for unsteady fluid flow and heat transfer. Int. J. Heat Mass Tran. 80, 812–824.

Vasheghani Farahani, M., Hassanpouryouzband, A., Yang, J., Tohidi, B., 2020. Heat transfer in unfrozen and frozen porous media: experimental measurement and pore-scale modeling. Water Resour. Res. 56 (9), e2020WR027885.

Woods, A.W., 2015. Flow in Porous Rocks. Cambridge University Press.

Yoon, H., Kang, Q., Valocchi, A.J., 2015. Lattice Boltzmann-based approaches for pore-scale reactive transport. Rev. Mineral. Geochem. 80 (1), 393–431.

Yoon, H., Valocchi, A.J., Werth, C.J., Dewers, T., 2012. Pore-scale simulation of mixing-induced calcium carbonate precipitation and dissolution in a microfluidic pore network. Water Resour. Res. 48 (2).

Yoshino, M., Inamuro, T., 2003. Lattice Boltzmann simulations for flow and heat/mass transfer problems in a three-dimensional porous structure. Int. J. Numer. Methods Fluid. 43 (2), 183–198.

Yu, Z., Fan, L.-S., 2009. An interaction potential based lattice Boltzmann method with adaptive mesh refinement (AMR) for two-phase flow simulation. J. Comput. Phys. 228 (17), 6456–6478.

Zhang, D., Li, S., Li, Y., 2021. Numerical investigation on acidic hydrothermal reactive flow in fractured rocks using a modified LBM model. Sustain. Energy Technol. Assessments 48, 101585.
Zhang, L., Kang, Q., Chen, L., Yao, J., 2016. Simulation of flow in multi-scale porous media using the lattice Boltzmann method on Quadtree grids. Commun. Comput. Phys. 19 (4), 998–1014.
Zhang, X., Bengough, A.G., Deeks, L.K., Crawford, J.W., Young, I.M., 2002. A novel three-dimensional lattice Boltzmann model for solute transport in variably saturated porous media. Water Resour. Res. 38 (9), 6-1–6-10.